Nuclear Engineering and Technology 48 (2016) 847–858

Available online at ScienceDirect

Nuclear Engineering and Technology

journal homepage: www.elsevier.com/locate/net

Invited Article

Bubbly, Slug, and Annular Two-Phase Flow in Tight-Lattice Subchannels

Horst-Michael Prasser [a,b,*], *Christian Bolesch* [a], *Kerstin Cramer* [a,c], *Daisuke Ito* [a,d], *Petros Papadopoulos* [a], *Abhishek Saxena* [a], *and Robert Zboray* [b]

[a] *ETH Zurich, Department of Mechanical and Process Engineering (D-MAVT), ML K13, Sonneggstrasse 3, CH-8092, Zurich, Switzerland*

[b] *Paul Scherrer Institute, PSI, 5232 Villigen PSI, Switzerland*

[c] *Université du Luxembourg, Campus Kirchberg, 6, rue Richard Coudenhove-Kalergi, L-1359, Luxembourg*

[d] *Kyoto University, Research Reactor Institute, 2-1010 Asashiro-nishi, Kumatori-cho, Sennan-gun, Osaka, 590-0494, Japan*

ARTICLE INFO

Article history:
Received 18 June 2016
Accepted 20 June 2016
Available online 25 June 2016

Keywords:
Computational Fluid Dynamics
Subchannel Flow
Tight Fuel Rod Lattice
Tomography
Two-Phase Flow
Void Fraction

ABSTRACT

An overview is given on the work of the Laboratory of Nuclear Energy Systems at ETH, Zurich (ETHZ) and of the Laboratory of Thermal Hydraulics at Paul Scherrer Institute (PSI), Switzerland on tight-lattice bundles. Two-phase flow in subchannels of a tight triangular lattice was studied experimentally and by computational fluid dynamics simulations. Two adiabatic facilities were used: (1) a vertical channel modeling a pair of neighboring subchannels; and (2) an arrangement of four subchannels with one subchannel in the center. The first geometry was equipped with two electrical film sensors placed on opposing rod surfaces forming the subchannel gap. They recorded 2D liquid film thickness distributions on a domain of 16 × 64 measuring points each, with a time resolution of 10 kHz. In the bubbly and slug flow regime, information on the bubble size, shape, and velocity and the residual liquid film thickness underneath the bubbles were obtained. The second channel was investigated using cold neutron tomography, which allowed the measurement of average liquid film profiles showing the effect of spacer grids with vanes. The results were reproduced by large eddy simulation + volume of fluid. In the outlook, a novel nonadiabatic subchannel experiment is introduced that can be driven to steady-state dryout. A refrigerant is heated by a heavy water circuit, which allows the application of cold neutron tomography.

1. Introduction

Light water reactors dominate the fleet of nuclear power plants worldwide. They have reached technological maturity and, with the introduction of the generation III, there has been tremendous progress with regard to safety compared to early prototypes and currently operated units. There are several authors exploring the opportunities to harden the neutron

* *Corresponding author.*
E-mail address: hprasser@ethz.ch (H.-M. Prasser).
http://dx.doi.org/10.1016/j.net.2016.06.007

spectrum in light water reactors by reducing the moderator-to-fuel ratio. The idea of using a boiling water reactor (BWR) as the basis of such a development is obvious: due to the formation of vapor, the density of the moderator is already significantly reduced, which is a good starting point. Yamashita et al [1] propose to further reduce moderation by applying a dense triangular lattice, which leads to hexagonal fuel elements and the use of Y-shaped control rods. They call this reactor the reduced moderation water reactor (RMWR). A conceptual design of such a reactor was published by Uchikawa et al [2]. The authors point out that the achieved neutron spectrum is hard enough to be suitable for iso-breeding with mixed oxide fuel. At the same time, it was found that the void coefficient of the lattice still stays slightly negative. Fukaya et al found a favorable effect of the harder neutron spectrum on the nuclide vector of the spent fuel [3]. A thermal hydraulic feasibility study was published by Liu et al [4]. The most recent status report we have found was issued by the Japan Atomic Energy Agency [5]. It seems to us that the RMWR may become a serious competitor to fast reactors with alternative coolants developed within the Gen-IV initiative.

In our opinion, reducing the moderation in a BWR is the most intriguing concept among similar ideas that can be found in literature. It is superior to dense lattice pressurized water reactors, such as the light water high conversion reactor investigated at the Paul Scherrer Institute (PSI), Switzerland, in the 1980s [6], where emergency cooling may become more difficult. Other authors propose the use of heavy water in a lattice typical for normal light water reactors [7]. This is another approach to harden the neutron spectrum, which is an effect of the much higher traveling length of neutrons in D_2O compared to H_2O. Still, it is an extremely costly approach. In our work, we therefore focused on the thermal hydraulics of narrow triangular subchannels with a certain emphasis put on the annular flow regime. The stability of the water film in high-void regimes, found in the upper part of the fuel elements of an RMWR is very likely the key issue when it comes to the coolability. Functional spacers with vanes for the flow control may play an important role in enhancing the heat removal, therefore the study of their influence on the liquid film was the main focus for most of our tests.

In view of the existing interest in the use of dense fuel rod lattices in BWRs, the Laboratory of Nuclear Energy Systems at ETH Zurich (ETHZ), Switzerland in cooperation with the Laboratory of Thermal Hydraulics at the PSI decided to launch two-phase flow studies in narrow triangular subchannels. The related work was started in 2010 as part of internally funded experimental and theoretical activities dealing with the flow structure in subchannels of rod bundles in general. Small budgets and limited personnel resources made is necessary to restrict the work to small-scale test facilities. Nonetheless, the availability of high-resolution instrumentation has resulted in detailed experimental data that provides deep insights into several flow phenomena occurring in the investigated channel geometries. The test data is used for the theoretical modeling which is conducted in the frame of PhD and masters projects.

2. Preliminary experiments in a flat narrow channel

Our first tests in narrow channels were performed in a vertical duct of rectangular cross-section with a high aspect ratio (Fig. 1) [8,9]. The flow cross-section was 32 mm wide, formed by two flat surfaces equipped with flat electrical film thickness sensors [10]. The gap width was 1.5 mm and the channel was

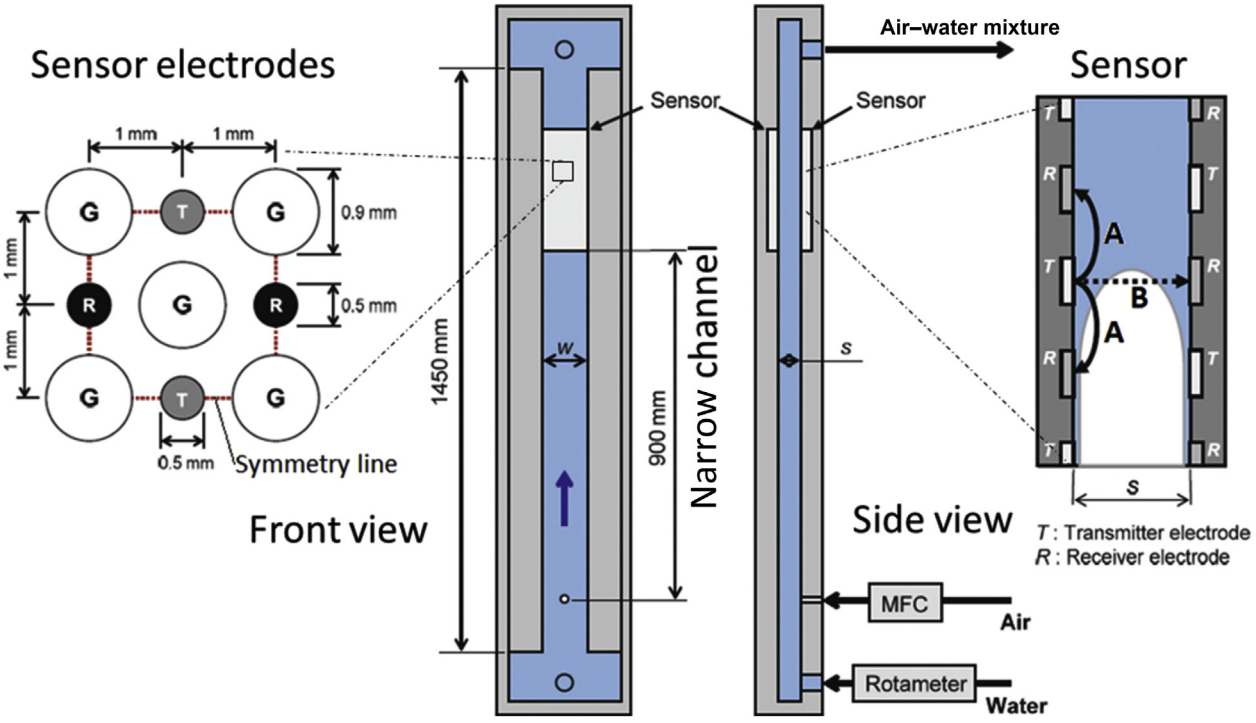

Fig. 1 – Vertical narrow channel with electrodes of the electric film sensor [8].

1450 mm tall. The fluids were water and air at ambient conditions, which were injected at the bottom of the test section. Each electrical film sensor consisted of a matrix of electrodes placed flush to the wall surface. In this way, the measurement was nonintrusive. Sequences of two-dimensional film thickness distributions were recorded with both sensors operating synchronously at a rate of 10 kHz. The lateral and vertical resolution was equal to 2 mm, defined by the pitch of the electrode matrix. The measuring range of the film thickness was from 0 μm to 600 μm with an uncertainty of approximately 10 μm. For more details please refer to the aforementioned publications [8–10].

A specific feature of the sensor system consisted of a combination of a conductance measurement between adjacent electrodes of each sensor alone, along with a measurement of the conductance between a transmitter electrode on one sensor and a receiver electrode on the opposite one. The signals of the first kind characterize the liquid film thickness covering the corresponding sidewall of the channel, while the measurement across the gap width can be used to detect water slugs that establish an electrical contact between the front and back sides of the channel.

The main innovation of the narrow channel experiments consists of the fast measurement of two-dimensional liquid film thickness distributions remaining underneath the gas bubbles, especially under very large gas plugs. The interest in characterizing this residual liquid film is connected to the extent it is able to sustain the heat removal from the rod surface. The results demonstrate a large degree of surface wetting even in the case of quite large gas plugs and despite the small gap width (Fig. 1). This information is taken from the conductance measured between electrodes of the sensor on either the front side or the back side of the channel alone (current path A in Fig. 1). As shown in Fig. 2, draining wave structures are often found in large rising gas agglomerates, especially in experiments in the churn flow region. The normalized conductance between electrodes of both opposite sensors subtracted from unity (current path B in Fig. 1) is interpreted as the instantaneous void fraction in the center of the channel. This signal turns to unity when the current is interrupted, while there is still liquid in the cross-section of the duct, as indicated by the film thickness signal. Both signals were used to approximately reconstruct the three-dimensional bubble shape [9].

A very interesting finding of the experiments in the narrow channel is the existence of dimpled liquid films. They were observed both in the case of small cap bubbles and larger gas plugs (Fig. 3). At the same time, the film thickness profile along the vertical center line was found to be more or less flat.

Finally, a comprehensive analysis of the patterns in time-average film thickness, void fraction, interfacial area concentration, and bubble velocity was performed over the range of gas and liquid flow rates that covered the range from bubbly to annular flow [9].

2.1. *Double subchannel models*

The concept of studying the annular flow established in the upper part of a BWR fuel element by using a double subchannel geometry was first developed by Damsohn [10]. A pair of adjacent subchannels in a rectangular fuel rod lattice was modeled by carving the profile out of a pair of Perspex plates (Fig. 4). Measurements were performed with electrical liquid film sensors, similar to the ones presented in Fig. 1A, but manufactured on a flexible printed circuit board. This allowed us to fix them on the surface of one of the fuel rods, of which 50% are half-cylinders, as shown in Fig. 4A. The double subchannel geometry allows the study of the flow in the subchannel itself, as well as in the connecting gap between two subchannels. The setup was used to examine the influence of spacer grids with vanes for the flow control. Some instantaneous wave patterns, as they were recorded by Damsohn, are shown in Fig. 4B. The time-averaged film thickness profiles show a very clear influence of spacer vanes (Fig. 4C).

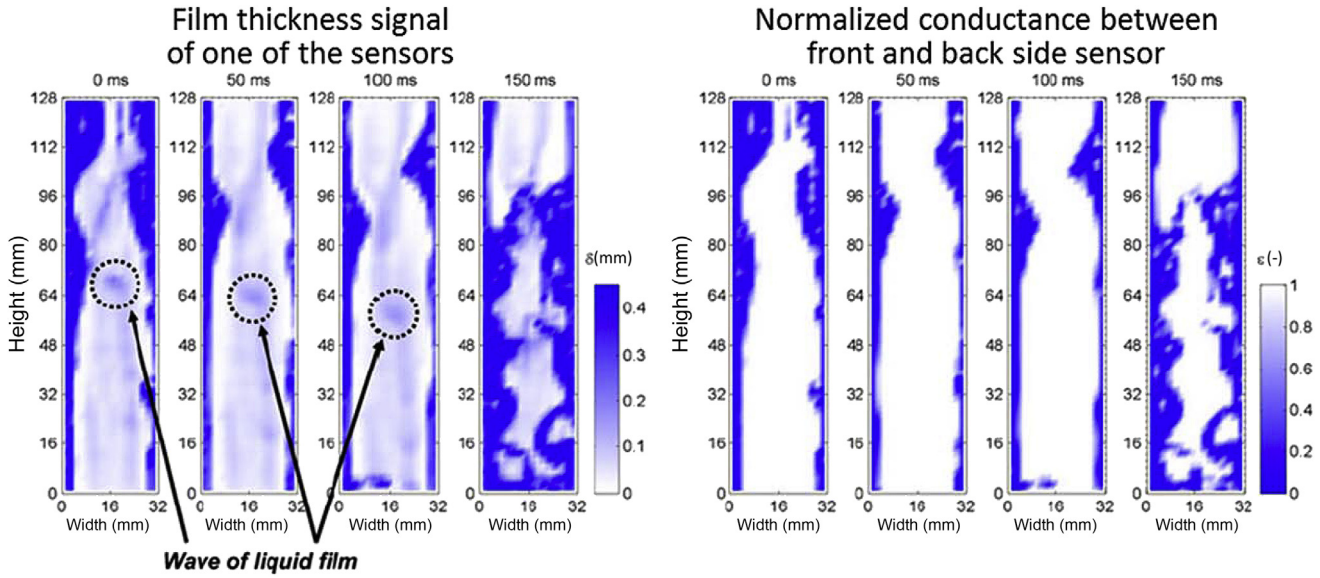

Fig. 2 – Sensor signals in a churn flow case at $J_G = 1.7$ m/s and $J_L = 0.347$ m/s [8]. J_G, superficial gas velocity, volume flux of the gaseous phase (m/s); J_L, superficial liquid velocity, volume flux of the liquid phase (m/s).

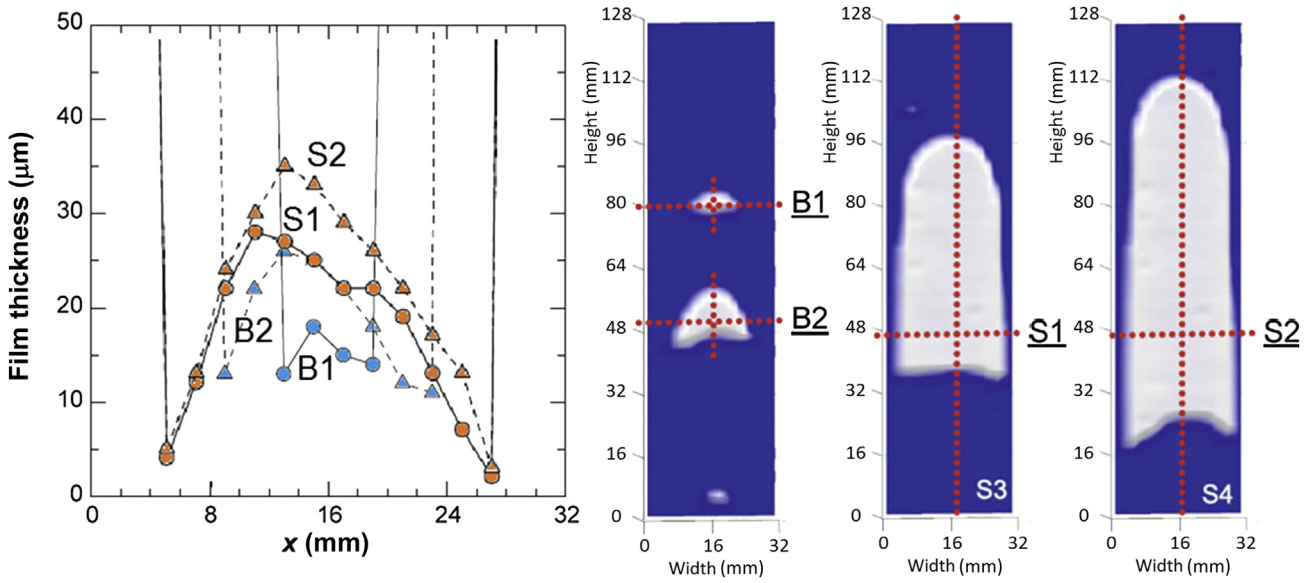

Fig. 3 – Horizontal film thickness profiles found in smaller cap bubbles (B) and large gas plugs (S) [8].

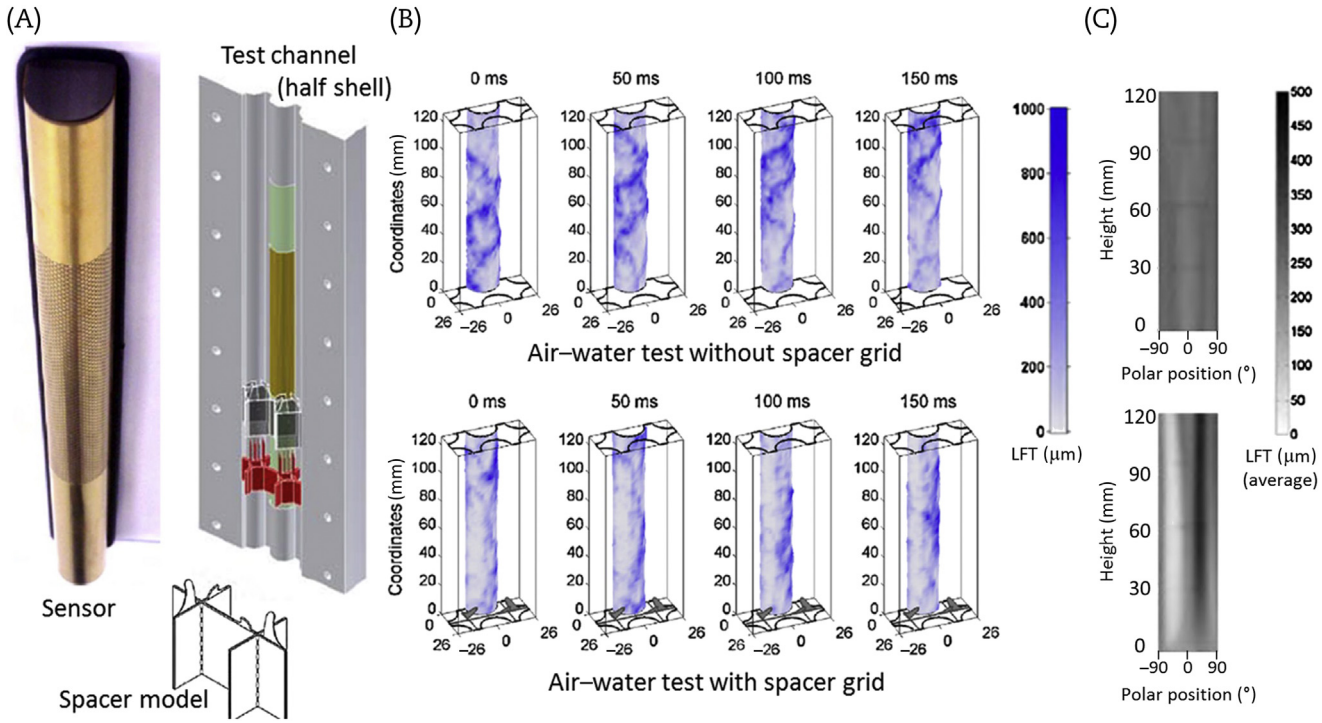

Fig. 4 – Using a double subchannel geometry to study the annular flow. (A) Sensor and a square lattice test channel. (B) Examples of instantaneous film thickness distributions. (C) Time-averaged film thickness profiles with and without spacer effect, measured in the double subchannel model (40 m/s air, 0.3 m/s water, vane angle 30 degree [11]).

Results obtained with the electric film sensor were confirmed by cold neutron tomography [12]. For this purpose, a test channel with a geometry identical to the flow duct shown in Fig. 4 was equipped with a mechanism for a slow rotation around the vertical axis and put into the cold neutron beam of the ICON facility at the spallation neutron source SINQ at the PSI.

Time-averaged film thickness distributions were extracted from three-dimensional tomographic data obtained during approximately 3 hours of acquisition of projections. Circumferential film thickness profiles show again very clearly the effect of the spacer vanes and a nearly perfect match with the film sensor data was found (Fig. 5).

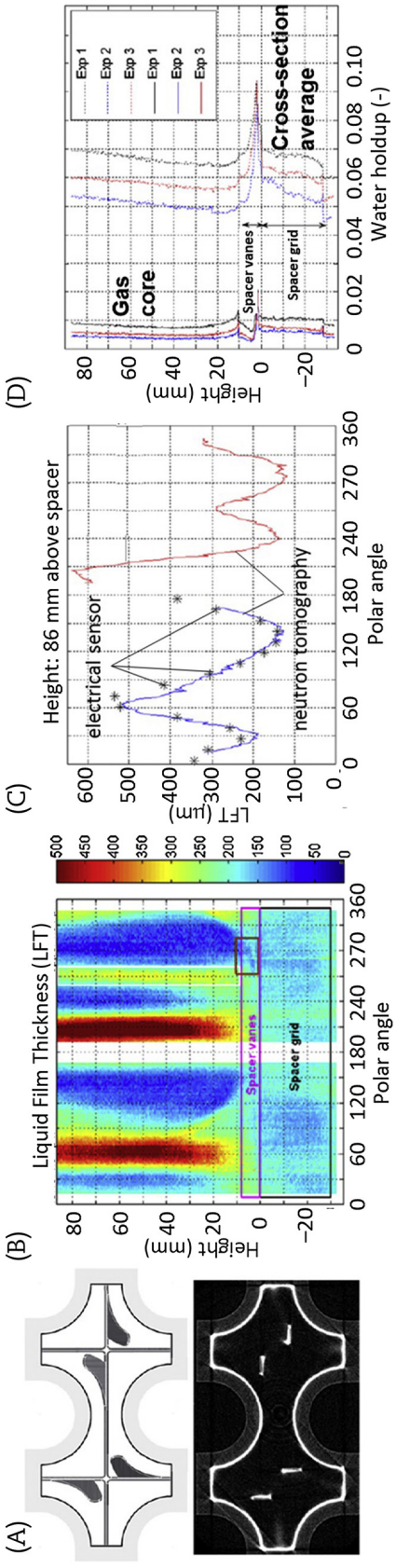

Fig. 5 – Tomography with cold neutrons in a double-subchannel model of a square lattice bundle. (A) Duct cross-section with spacer top view. (B) Liquid film thickness distribution extracted from a 3D tomographic image. (C) Comparison of the circumferential film thickness profile with the electrical film sensor. (D) Axial liquid holdup profiles [12]. Exp, experiment; LFT, liquid film thickness.

Neutron tomography and electrical film sensor complement each other. With a sampling frequency of 10 kHz, the electrical sensor is by a factor of 10^8 faster than cold neutron tomography, which has to rely on the slow mechanical rotation of the object under the beam. This means that the electrical sensor is capable of displaying fast transient structures, such as wave patterns passing by, while the neutron tomography has a higher spatial resolution and provides information not only from the surface of the instrumented fuel rod model, but from everywhere in the cross-section. In this way, the liquid holdup was quantified as an average over the cross-section of the subchannel and in the gas core separately. This means that quantitative information on droplet entrainment can be provided (Fig. 5D). This feature is interesting from the point of view of average void data necessary for the determination of the neutron kinetic feedback.

After the success in studying the annular flow in a rectangular geometry, the double subchannel concept was applied to a pair of adjacent subchannels formed by four fuel rods arranged in a dense triangular lattice [13]. In these experiments, a pair of electrical film sensors were mounted opposite each other, as shown in Fig. 6, quite similar to the experiments in the flat narrow gap described above.

Again, the pair of liquid film sensors were capable of recoding the water film underneath the gas bubbles with a high spatial (2 mm) and temporal (0.1 ms) resolution. The evaluation of the electrical signal traveling from one sensor to the other showed that the connection between opposite fuel rod surfaces is interrupted when the annular flow regime is reached (Fig. 7). The contact via the liquid phase is still perfect in the liquid slugs between Taylor bubbles. It starts to deteriorate soon, when the gas flow rate reached values characteristic for the churn turbulent flow regime. Despite this, the wave patterns found on both opposing surfaces are still quite synchronized.

3. Neutron tomography in an arrangement of four subchannels

In the double subchannel geometry described above, both of the subchannels have two nonrealistic no-slip boundaries on the symmetry lines, along which the pair of channels is cut out of the triangular lattice [15]. For the tomography with cold neutrons, a channel geometry was developed, which represents a subchannel without such unrealistic no-slip conditions. It consists of four subchannels, from which the central one is connected to three neighboring ones via correctly modeled subchannel gaps. Only the three peripheral subchannels have two nonrealistic no-slip boundaries each at the cut connections to the rest of the lattice (Fig. 8). In our opinion, this is an optimal configuration for a model geometry that has to be restricted to a small part of the entire fuel bundle cross-section for practical reasons.

An example of the measured time-averaged film thickness distribution along all three surfaces of the central subchannel is shown in Fig. 9. The image is a result of an evaluation of the three-dimensional reconstruction of the liquid holdup distribution inside the flow channel. The 3D tomogram is obtained from a complete set of two-dimensional projections, i.e., from the radiograms recorded by the neutron camera during

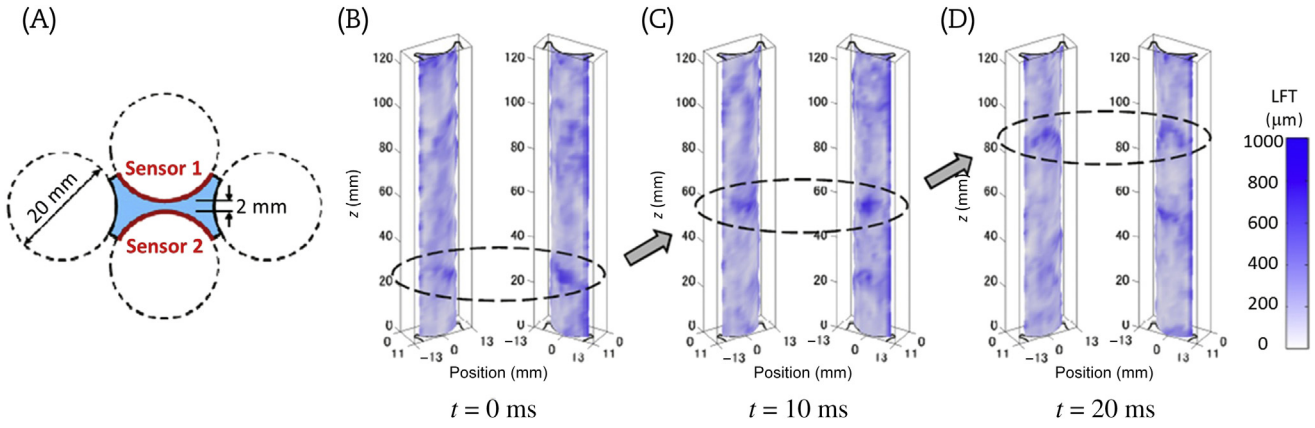

Fig. 6 – Instantaneous liquid film thickness distribution in the tight-lattice subchannel ($J_G = 60$ m/s and $J_L = 0.2$ m/s, [13]). J_G, superficial gas velocity, volume flux of the gaseous phase (m/s); J_L, superficial liquid velocity, volume flux of the liquid phase (m/s).

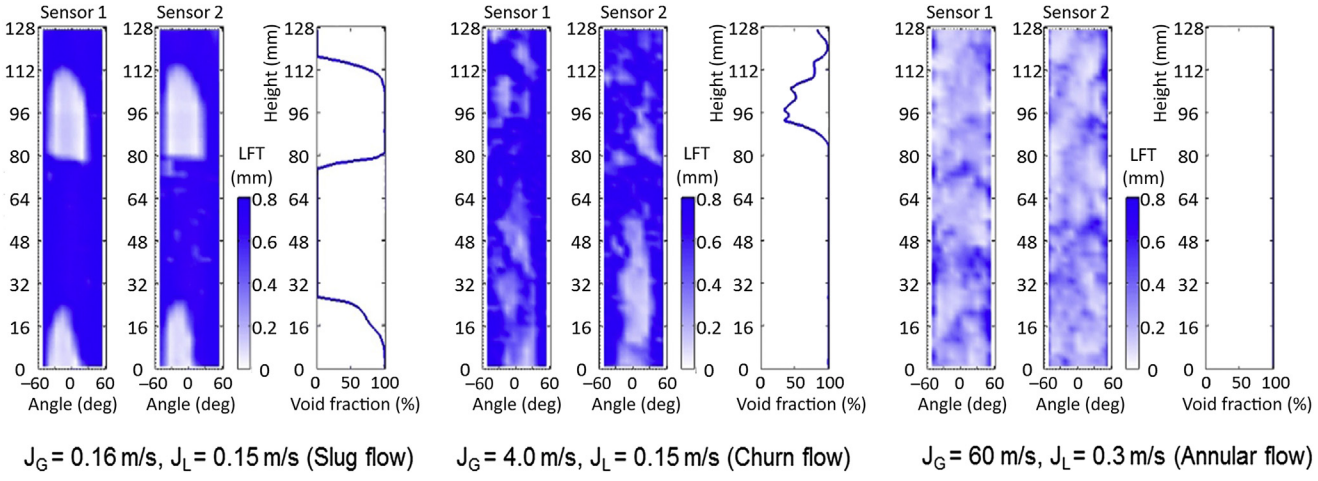

Fig. 7 – Instantaneous film thickness distributions and the conductance signal between the opposite sensors (void fraction) at different flow regimes [14].

turning of the object around an angle of 180 degrees. The distribution of the liquid phase is found by subtracting the image of the empty channel from the image obtained in the presence of the two-phase flow. As visible in the corresponding differential tomographic image shown in Fig. 8D, the liquid phase is concentrated on the inner surface of the flow duct. The film thickness is found by integrating the reconstructed neutron attenuation along the chords shown with a yellow color in Fig. 8D. More details are available in the study conducted by Zboray and Prasser [15].

The film thickness profiles shown in Fig. 9 clearly show the influence of the spacer model equipped with three vanes. There is a stripe of low film thickness pointing in the direction of the tips of the vanes. This is caused by the high shear stress imposed by the accelerated gas flow. In the low-velocity region affected by the shadow of the vane, the film thickness is high. Differences in the profiles on the three fuel rod surfaces are a result of positioning tolerances of the spacer model. They show the strong sensitivity of the flow to small asymmetries of the geometry.

4. Computational fluid dynamics modeling of annular film flows in subchannels

Our first attempt to calculate the time-averaged film thickness distribution along the surface of a fuel rod and its modulation by the presence of a spacer grid with vanes was based on a strongly simplified two-dimensional liquid film model coupled to a steady-state Reynolds-averaged Navier–Stokes simulation of the flow field in the gas core of the annular flow [16]. The gas phase was assumed to flow without an influence of the present liquid film. The geometry of the channel including the spacer was reflected by detailed meshing. From the results of the computational fluid dynamics calculation, the shear stress distribution at the no-slip boundaries was exported and used as an input for a simple algebraic film model derived on basis of the assumption of a laminar flow in the film. The model contained a two-dimensional mass conservation equation in order to represent the transport of the liquid driven by the gas core. The

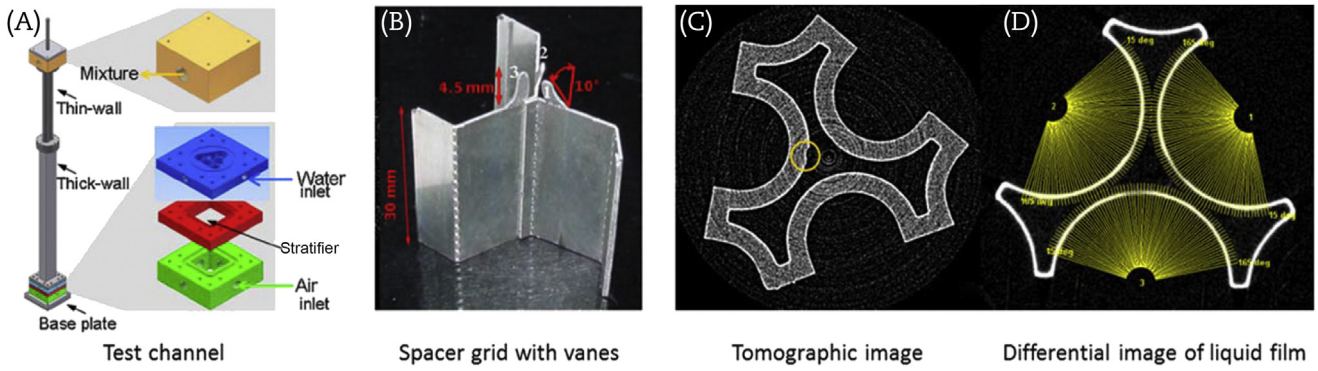

Fig. 8 – Turnable test channel for the tomography. (A) With cold neutrons. (B) Tested spacer geometry. (C) Tomographic image of a selected measuring cross-section above the spacer vanes. (D) The resulting differential image displaying the liquid film with integration chords (yellow) for the film thickness estimation [15].

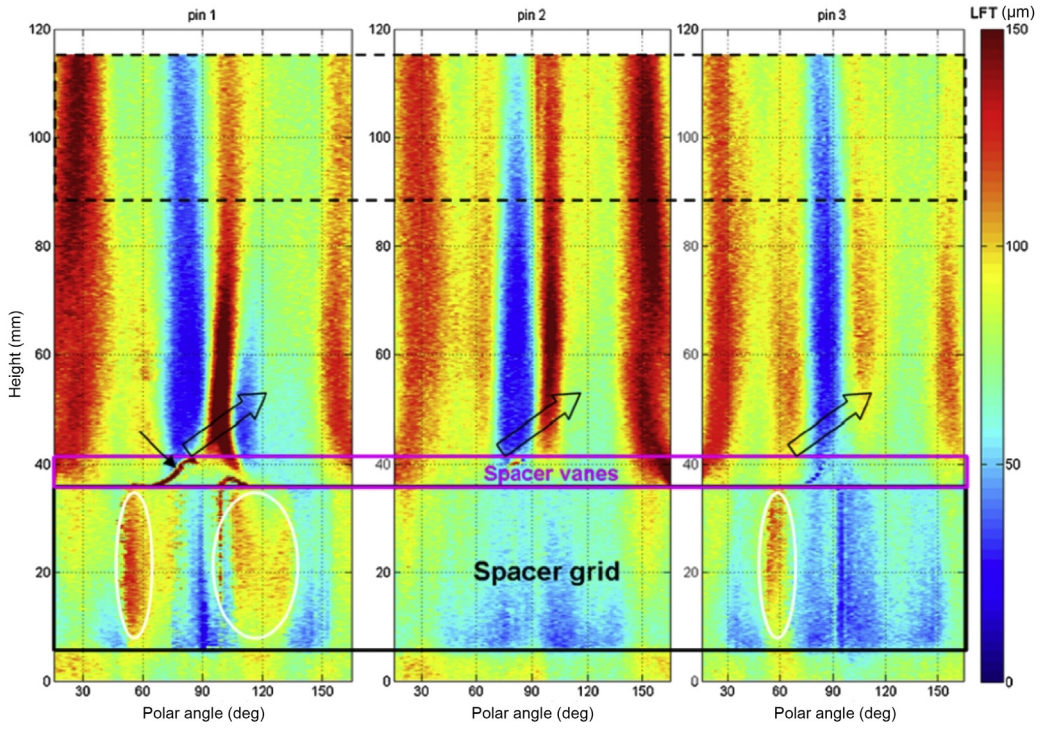

Fig. 9 – Film thickness distribution on all three fuel pins from the reconstructed tomographic images ($J_G = 34.74$ m/s, $J_L = 0.60$ m/s, small arrow: water accumulation on spacer vane; large arrows: direction of swirl induced by spacer vanes) [15]. J_G, superficial gas velocity, volume flux of the gaseous phase (m/s); J_L, superficial liquid velocity, volume flux of the liquid phase (m/s); LFT, liquid film thickness.

film thickness and the advection velocity were calculated using the local shear stress and a virtual viscosity, which was treated as an empirical parameter and fitted to the experimental results from the tests without the spacer grid. After this initial adjustment, the model was very well able to predict the film thickness distribution in the presence of the spacer grid reasonably without any further adjustment of the empirical coefficients. The introduction of an empirical dispersion coefficient and a virtual surface tension, both smoothing out to steep film thickness gradients, improved the results gradually.

The main drawback of this approach consists in the accumulation of liquid mass in points of low shear stress. This was overcome by the addition of a 2D momentum conservation equation of the liquid in the film to the model [17]. Portions of liquid arriving at points of low-driving shear stress are now able to propagate further by their inertia. Saxena [17] first applied this model to a rectangular geometry. A future change to a triangular lattice can be easily performed. Recently, the model of Saxena was extended by a mass sink term representing the phase transition in case of a heat supply from the wall. First results were obtained

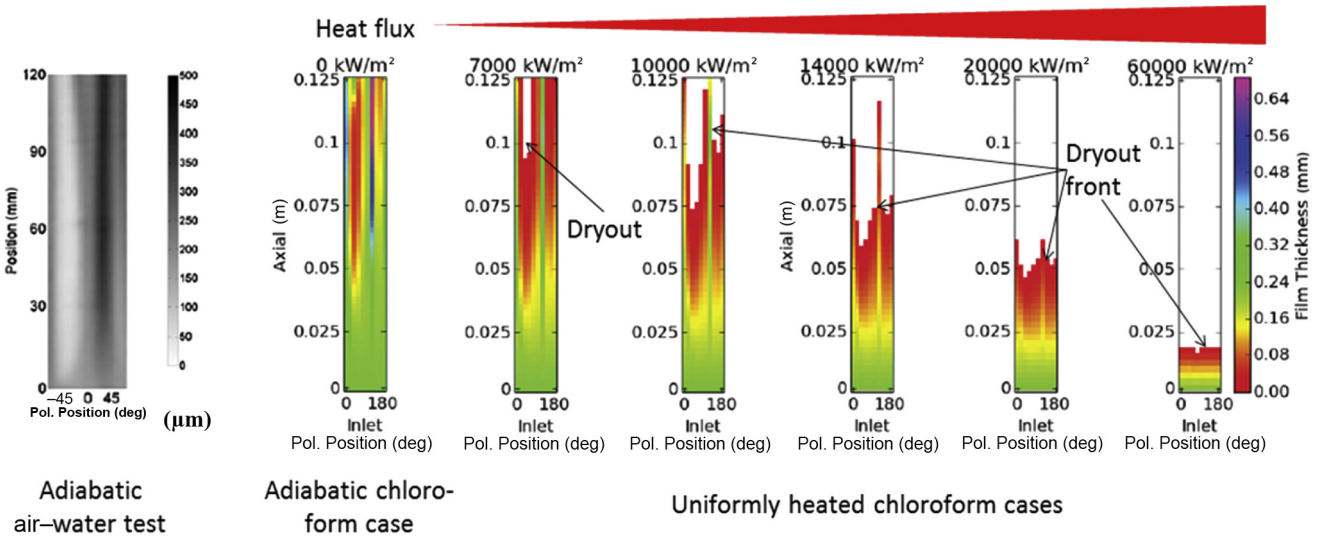

Fig. 10 – Results of the steady-state film flow model based on a 2D Navier–Stokes equation for the liquid phase, coupled to a steady-state 3D RANS model of the gas core by the shear stress distribution for different uniform heat fluxes, starting from the adiabatic case [17, 18], fluid: $CHCl_3$; inlet film thickness: 240 μm; $J_L = 0.1$ m/s; $J_G = 30$ m/s. J_G, superficial gas velocity, volume flux of the gaseous phase (m/s); RANS, Reynolds-averaged Navier–Stokes; J_L. superficial liquid velocity, volume flux of the liquid phase (m/s).

for a uniform distribution of the heat flux on the fuel rod surface [18].

The model is able to predict the shape of the dryout front. In the absence of a spacer, the front is nearly flat. The modulation of the film thickness and the velocity profiles by a spacer with vanes leads to a curved dryout line, as shown in Fig. 10. A comparison of the adiabatic case, which corresponds to the model of Saxena [17] before the extension by Cramer [18], is shown on the left side of Fig. 10. The calculation was carried out with chloroform as the working fluid because this will be used in future experiments for the model validation (see next section). The experimental distribution shown in the figure was an air–water experiment, therefore the comparison can be only qualitative. Still, the overall structure of the film and in particular the angular positions of streaks of large and small film thickness are well predicted. The results await experimental validation, which is due soon.

A second approach pursued in our group is the application of a large eddy simulation coupled with an interface tracking technique, in our case with the volume-of-fluid approach. This time, the triangular geometry of the dense lattice was chosen. The narrow space can be more easily reflected by a sufficiently fine grid for the simulation (Fig. 11). Saxena managed to reproduce the film thickness profiles measured by cold neutron tomography quite well [19]. Fig. 11 shows the comparison of circumferential film thickness profiles with the cold neutron tomography measurement. The calculation is reproducing measurement in a satisfying way; the main tendencies of the shape of the distribution are well reproduced, whereas some quantitative discrepancies are evident. A

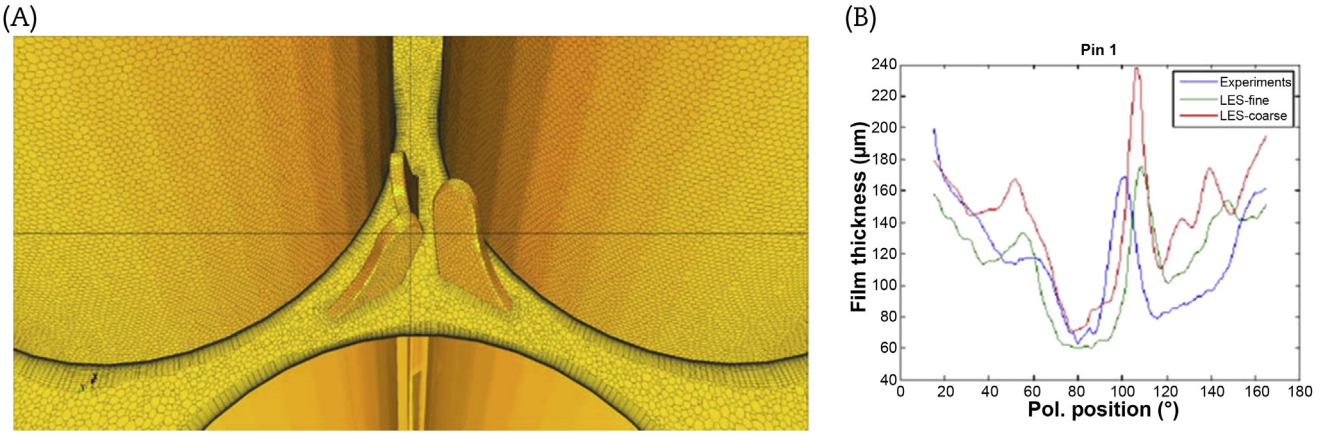

Fig. 11 – Computational grid. (A) For the fine mesh calculation. (B) Obtained time-averaged liquid film thickness distributions on Pin 1, spatially averaged from 10–40 mm downstream of spacer using a coarse and fine mesh [19]. LES, large eddy simulation.

convergence towards the measuring results was found in a mesh refinement study.

A highlight of the study is the measurement and the theoretical prediction of the liquid film distribution on the spacer vanes (Fig. 12). The higher accumulation of water on the downstream face of the vane is very well modeled, also the overall distributions are matching, at least qualitatively.

5. Outlook: experiments in nonadiabatic film flows

As a next step, nonadiabatic experiments in a heated model of a subchannel are in preparation [20]. The work is being carried out in the frame of a PhD project. The most important details are illustrated in Fig. 13. A single subchannel corresponding to a square lattice geometry is surrounded by four auxiliary channels to ensure that there is no unrealistic no-slip condition present in the subchannel gaps. The turnable test section is mounted in a scaffold, which can be put both into the shielding hut of the cold neutron imaging facility ICON at PSI and in an X-ray imaging facility at ETHZ. As shown in Fig. 13, it consists of two subsequent heated sections, the power of which can be individually controlled. This is used to set the desired inlet conditions for the upper section, which is the actual measuring section that will be put in the beam.

The heated fluid is chloroform ($CHCl_3$). This has the advantage of a low boiling point and a low latent heat of evaporation and allows the use of water at ambient pressure as a heating fluid, which has a high specific heat capacity. The heating by a fluid instead of electrical heaters eliminates the danger of a burnout. We hope to be able to establish a steady-state dryout front, which can be visualized by the mentioned tomographic imaging methods. The boiling point of chloroform at ambient pressure is 61.2°C, while the water temperature is varied between 70°C and 100°C in order to control the heating power. The latter is provided by two electrical heaters in the water circuits of 6 kW each. The water is circulated at a flow rate of about 15 l/min, which is sufficient to keep the heat-up span low and the heat transfer coefficients from the side of the heating flow sufficiently high to guarantee a nearly isothermal heating of the chloroform. The flow scheme of the facility is also given in Fig. 13.

With regard to the resolution needed to identify the dryout front, cold neutron tomography is superior. It requires the use of heavy water as the heating fluid, because it has a

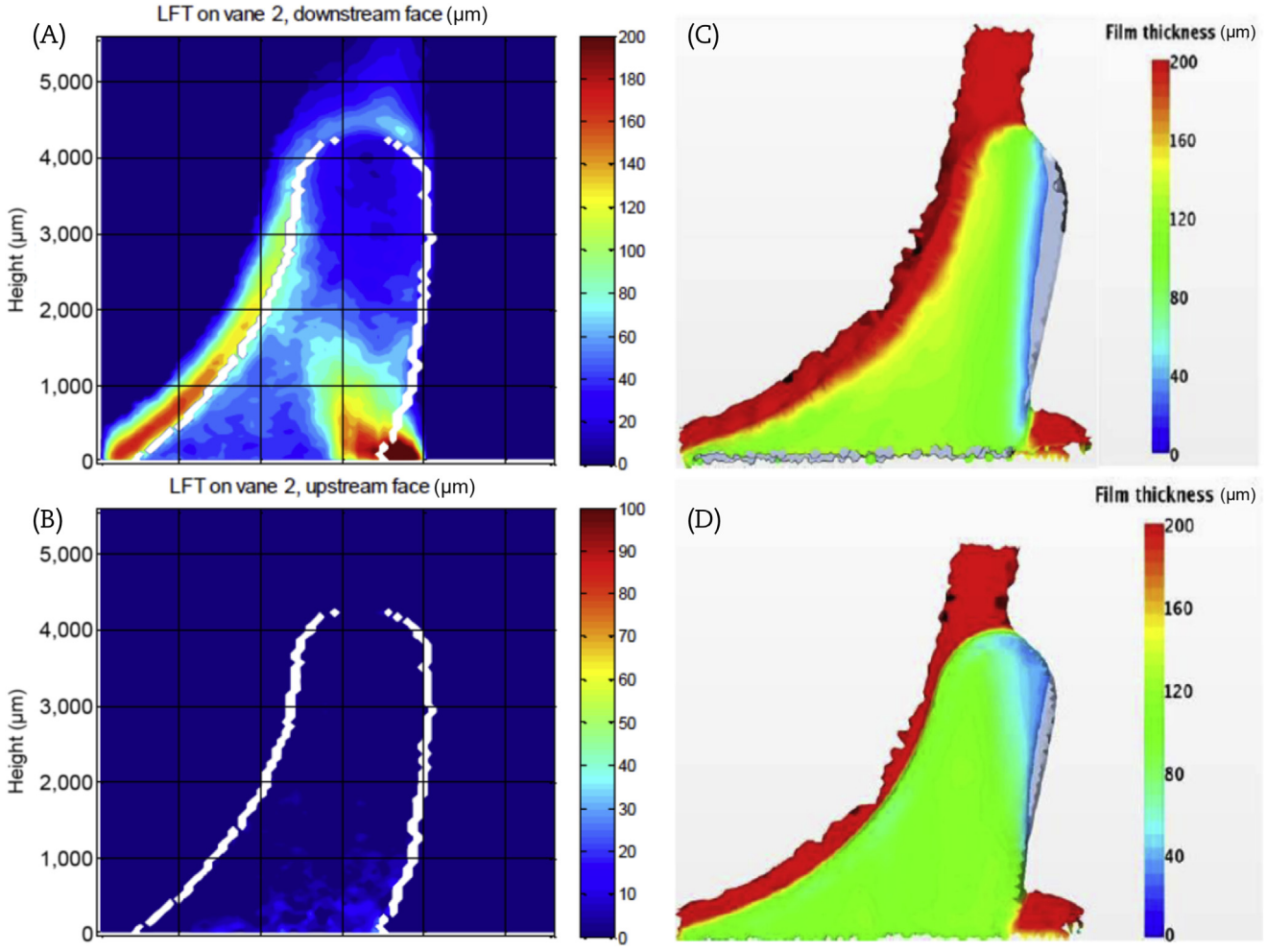

Fig. 12 – Liquid film thickness distribution on downstream and upstream faces of spacer vanes 2. (A) and (B) cold neutron tomography. (C) and (D) LES + VoF [19]. LES, large eddy simulation; LFT, liquid film thickness; VoF, volume-of-fluid.

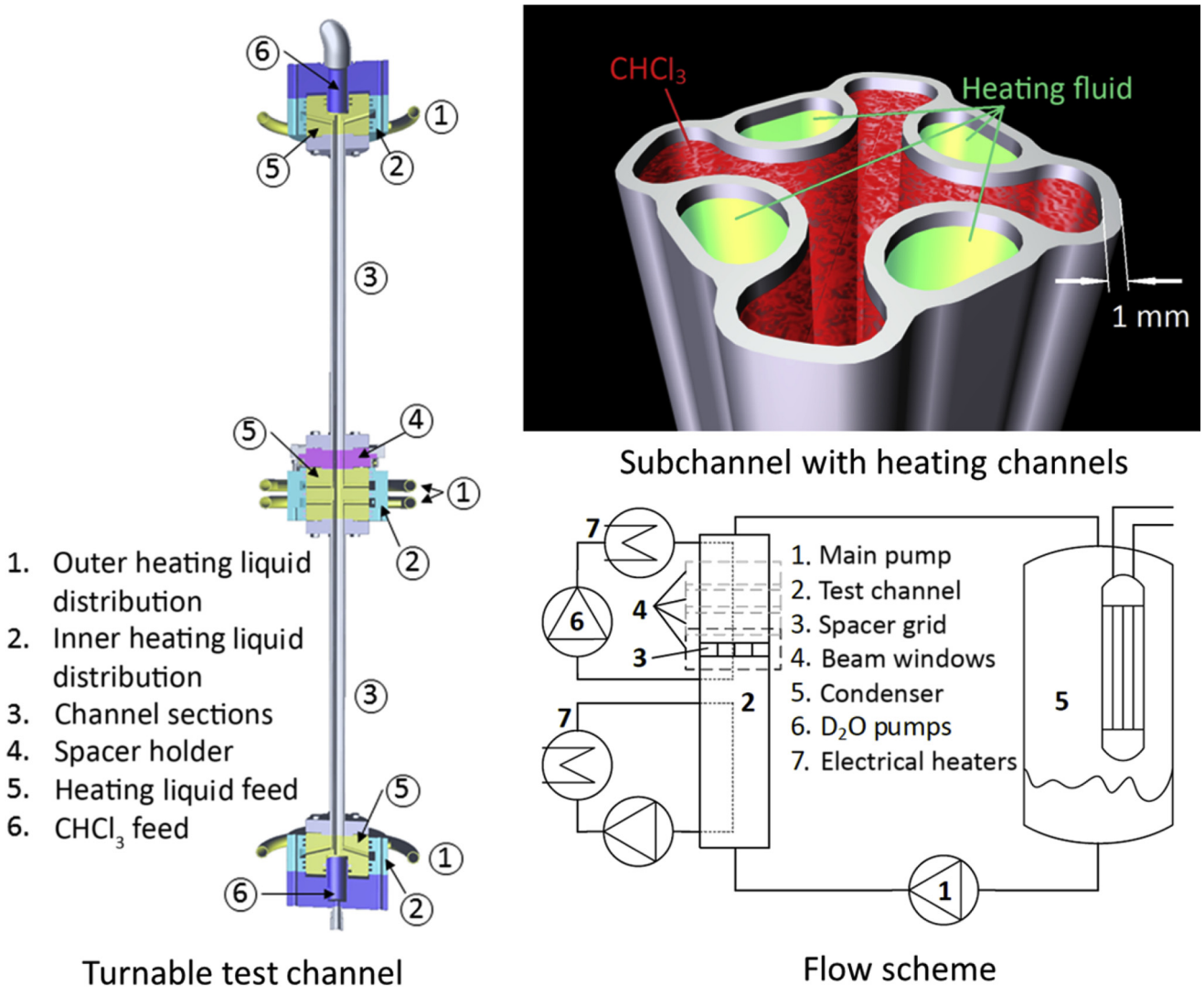

Fig. 13 – Test facility of the nonadiabatic subchannel experiment.

significantly lower attenuation due to a lower elastic scattering cross-section and a lower absorption cross-section compared to normal (light) water. This is necessary to reduce the negative influence of the heating channels on the imaging quality. Still, regimes with low void fraction cause a nearly complete attenuation of the cold neutron beam. X-ray imaging instead has the advantage of allowing the studies to extend to such low void fraction cases in the region of bubbly, slug and churn-turbulent flow regimes, because it is less attenuated and penetrates fluid of higher density. Furthermore, the use of the X-ray imaging station at ETHZ allows us to operate the facility in periods when there is no beam-time at the SINQ cold neutron source available.

The test facility was successfully commissioned in two series of experiments. The first experiments were carried out with an X-ray radiography setup, consisting of a standard X-ray generator and a two-dimensional detector array. The generator was operated at 80 kV in fluoroscopy mode at a current of 5 mA. First tomographic images were obtained using a filtered back projection method applied to a complete set of projections that were recorded by rotating the channel under the X-ray beam (Fig. 14A and 14B). The exposure time for each projection was 33.3 ms. The channel was rotated and images were taken from a full rotation. A tomographic image reconstruction was carried out first for the empty subchannels, together with the heating channels filled with H_2O. The corresponding image shows the aluminum of the channel walls as a stronger attenuating material than the water in the heating channels. After switching on chloroform flow and increasing the heating power until an annular flow regime was reached, a second set of projections was taken, the image reconstruction was carried out and the empty channel image was subtracted. The result shows the evaporating chloroform film. In the case of the cold neutrons, the experiment lasted much longer because the acquisition of a single projection lasts 20 seconds. The image shown in Fig. 14 was obtained by subtracting an image of the totally empty channel from the image taken at full operation. Both chloroform film and D_2O are visible.

The results are preliminary and can only be used as proof of principle. The next step consists of the realization of tests according to a well-defined test program. During the described shake-down tests, some corrosion of the aluminum in contact

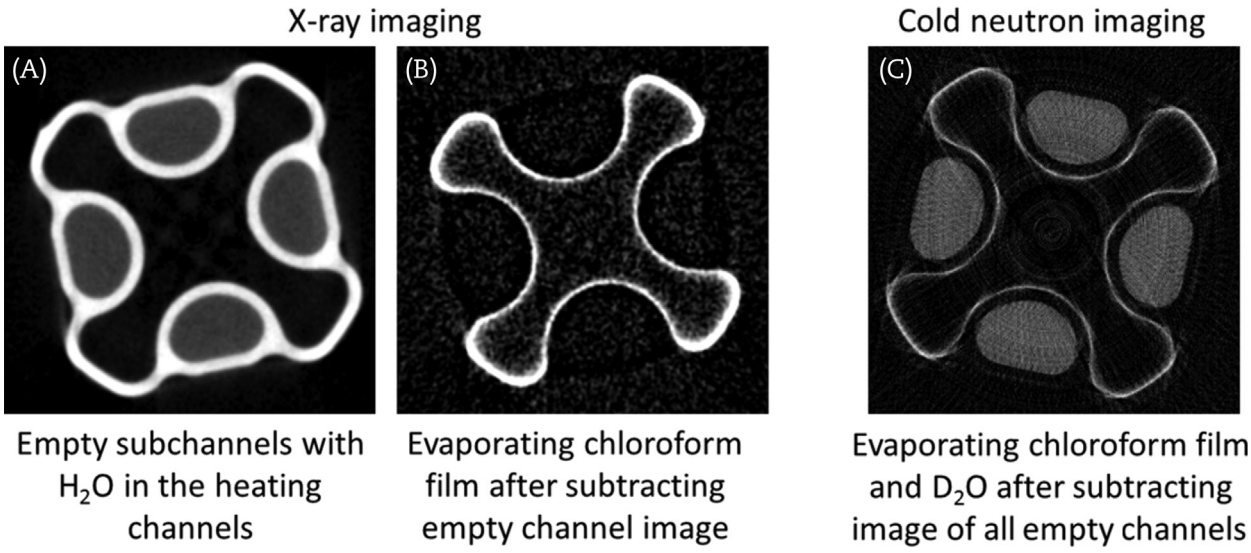

Fig. 14 – Tomographic images obtained from a full set of projections recorded by rotating the operating channel.

with the heated chloroform was observed, which made it necessary to improve the surface quality of the aluminum duct. The test facility can be modified to adopt a test channel with a triangular subchannel in the future.

6. Conclusion

In the paper, a short overview is given of the activities of the Laboratory of Nuclear Energy Systems at ETHZ in cooperation with the Laboratory of Thermal Hydraulics at the PSI. The developed instrumentation and the experimental techniques allow very detailed insights into the structure of the two-phase flow in the subchannels of square and triangular fuel rod lattices. Special attention is paid to the annular flow regime and to the influence of functional spacer grids with vanes for the flow control. Two modeling approaches based on Reynolds-averaged Navier–Stokes and large eddy simulation are in development and show promising first results. The presented methods are suitable tools for the optimization of fuel rod bundle geometries and especially of spacer geometries. This might be interesting for fuel element developers. Code developers could benefit from validation opportunities, as well as from the proposed concepts of film flow modeling.

Conflicts of interest

There is no conflict of interest. The work was performed by institutional funding of PSI and ETHZ. Results can be freely published.

REFERENCES

[1] J. Yamashita, F. Kawamura, T. Mochida, Next-generation nuclear reactor systems for future energy, Hitachi Rev. 53 (3) (2004) 131–135.

[2] S. Uchikawa, T. Okubo, T. Kugo, H. Akie, R. Takeda, Y. Nakano, A. Ohunki, T. Iwamura, Conceptual design of innovative water reactor for flexible fuel cycle (FLWR) and its recycle characteristics, J. Nucl. Sci. Technol. 44 (3) (2007) 277–284.

[3] Y. Fukaya, T. Okubo, S. Uchikawa, Investigation on spent fuel characteristics of reduced-moderation water reactor (RMWR), Nucl. Eng. Des 238 (2008) 1601–1611.

[4] W. Liu, A. Ohnuki, H. Yoshida, M. Kureta, K. Takase, H. Akimoto, Thermal feasibility analyses for the 1356MWe high conversion-type innovative water reactor for flexible fuel cycle, Heat Transfer Eng. 29 (8) (2008) 704–711.

[5] JAEA, Reduced-Moderation Water Reactor (RMWR), Status Report 80, release 04.04, JAEA., 2011. Available from: https://aris.iaea.org/sites/..%5CPDF%5CRMWR.pdf.

[6] R. Brogli, B. Kuczera, H. Moldaschl, W. Oldekop, Lessons learned from the PWHCR development, in: R. Chawla, R. Böhme, J. Dreier, R. Brogli, J. Axmann, H.D. Berger, C.H.M. Broeders, H. Hager, B. Kuczera, H. Moldaschl, W. Oldekop, S. Pelloni, N. Rouge, M. Schatz, R. Seiler, S. Yanar (Eds.), Contributions to Technical and Economic Aspects of High Converters, PSI-Bericht Nr. 71, Paul Scherrer Institut, June 1990, pp. 54–62.

[7] H. Tochihara, Y. Komano, M. Ishida, K. Narukawa, M. Umeno, Nuclear design for mixed moderator PWR, Prog. Nucl. Energ. 32 (314) (1998) 533–537.

[8] D. Ito, M. Damsohn, H.-M. Prasser, M. Aritomi, Dynamic film thickness between bubbles and wall in a narrow channel, Exp. Fluids 51 (3) (2011) 821–833. Available from: http://link.springer.com/article/10.1007/s00348-011-1105-3.

[9] D. Ito, H.-M. Prasser, Measurement of two-phase flow structure in a narrow rectangular channel, in: G.U. Beltrán, L.L. Castro Gómez (Eds.), Flow Measurement, InTech, 2012, pp. 73–94.

[10] M. Damsohn, H.-M. Prasser, High-speed liquid film sensor for two-phase flows with high spatial resolution based on electrical conductance, Flow Meas. Instrum. 20 (2009) 1–14.

[11] M. Damsohn, H.-M. Prasser, Experimental studies of the effect of functional spacers to annular flow in subchannels of a BWR fuel element, Nucl. Eng. Des. 240 (2010) 3126–3144.

[12] R. Zboray, J. Kickhofel, M. Damsohn, H.-M. Prasser, Cold-neutron tomography of annular flow and functional spacer performance in a model of a boiling water reactor fuel rod bundle, Nucl. Eng. Des. 241 (2011) 3201–3215.

[13] D. Ito, H.-M. Prasser, Spatio-temporal measurement of liquid film thickness in tight-lattice double subchannels, The 15th International Topical Meeting on Nuclear Reactor Thermal-Hydraulics, NURETH-15, Pisa, Italy, May 12–17, 2013, Paper NURETH15-226. Available from: http://www.ans.org.

[14] P. Papadopoulos, Measurements in a Triangular Tight Lattice Channel with Mesh Sensors, Bachelor Thesis, ETH Zurich, Laboratory of Nuclear Energy Systems., 2011. Available from: hprasser@ethz.ch.

[15] R. Zboray, H.-M. Prasser, Neutron imaging of annular flows in a tight lattice fuel bundle model, Nucl. Eng. Des. 262 (2013) 589–599.

[16] M. Damsohn, Liquid films and droplet deposition in a BWR fuel element, PhD Thesis No. 19527, ETH Zurich., 2011. Available from: http://e-collection.library.ethz.ch/eserv/eth:2835/eth-2835-02.pdf.

[17] A. Saxena, H.-M. Prasser, Liquid Film Modeling in BWR Subchannel with Spacers, Application of CFD/CMFD Codes to Nuclear Reactor Safety and Design and their Experimental Validation (CFD4NRS-5), OECD/NEA & IAEA Workshop, Zurich, Switzerland, September 9–11, 2014, paper S02–4. Available from: https://www.oecd-nea.org/nsd/csni/cfd.

[18] K. Cramer, Investigation of the Influence of the Phase Transition on the Liquid Film Thickness in Vertical, Annular Two-phase Flow, Master thesis, ETH Zurich., April 2014. Available from: hprasser@ethz.ch.

[19] A. Saxena, R. Zboray, H.-M. Prasser, Simulations and Measurements of Adiabatic Annular Flows in a Triangular, Tight Lattice Nuclear Fuel Bundle Model, Application of CFD/CMFD Codes to Nuclear Reactor Safety and Design and their Experimental Validation (CFD4NRS-5), OECD/NEA & IAEA Workshop, Zurich, Switzerland, September 9–11, 2014, paper S02–1. Available from: https://www.oecd-nea.org/nsd/csni/cfd.

[20] R. Zboray, Ch. Bolesch, H.-M. Prasser, Neutron and X-ray imaging techniques for nuclear fuel rod bundle optimization and development, SWINTH-2016, Livorno, June 15–17, 2016, paper 17. Available from: hprasser@ethz.ch.